International Journal of Modern Physics B
Vol. 32, No. 5 (2018) 1850043 (15 pages)

DOI: 10.1142/S0217979218500431

World Scientific
www.worldscientific.com

Bursting patterns and mixed-mode oscillations in reduced Purkinje model

Feibiao Zhan*, Shenquan Liu†,¶, Jing Wang‡ and Bo Lu§

School of Mathematics,
South China University of Technology,
Guangzhou 510640, P. R. China
**zhanfeibiao@yeah.net*
†*mashqliu@scut.edu.cn*
‡*wangjing901225@gmail.com*
§*cheersnow@163.com*

Received 12 July 2017
Revised 15 September 2017
Accepted 19 September 2017
Published 20 November 2017

Bursting discharge is a ubiquitous behavior in neurons, and abundant bursting patterns imply many physiological information. There exists a closely potential link between bifurcation phenomenon and the number of spikes per burst as well as mixed-mode oscillations (MMOs). In this paper, we have mainly explored the dynamical behavior of the reduced Purkinje cell and the existence of MMOs. First, we adopted the codimension-one bifurcation to illustrate the generation mechanism of bursting in the reduced Purkinje cell model via slow–fast dynamics analysis and demonstrate the process of spike-adding. Furthermore, we have computed the first Lyapunov coefficient of Hopf bifurcation to determine whether it is subcritical or supercritical and depicted the diagrams of inter-spike intervals (ISIs) to examine the chaos. Moreover, the bifurcation diagram near the cusp point is obtained by making the codimension-two bifurcation analysis for the fast subsystem. Finally, we have a discussion on mixed-mode oscillations and it is further investigated using the characteristic index that is Devil's staircase.

Keywords: Bursting; slow–fast dynamics; Lyapunov coefficient; mixed-mode oscillations.

PACS numbers: 02.30.Oz, 05.45.-a, 89.19.lj

1. Introduction

Purkinje cells are merely efferent neurons to spread action potentials in cerebellar cortex, which is critical to our coordinated motion. To research physiological

¶Corresponding author.

function of cerebellar Purkinje cells, there are some recent literatures to investigate the bistability *in vivo* and dynamical properties of Purkinje cells via experiments or theoretical studies.[1,2] Purkinje cell possesses "fold/homoclinic" bursting via "fold/homoclinic" hysteresis loop, and its bistability is intrinsic.[1] Reduced model inherited the bistability and certain dynamical behaviors of the original model. Therefore, we will investigate the reduced model which is necessary to understand the dynamical properties of Purkinje cell.

In many neuronal models,[3–7] the dynamical behavior of electrical activities has been explored using a variety of methods such as bifurcation theory, changing time delay, adding phase noise or electromagnetic radiation and so on, and we can see that the discharge rhythm transition mode was investigated deeply in some literatures.[8–11] Detailed bifurcation patterns of slow–fast dynamics analysis are researched in recent works[12–17] by using a specific model. Abundant nature of the discharge means that it possesses rich dynamical properties.[18,19] Che and his collaborators[20] have analyzed the codimension-one bifurcation, Zhao and Gu[21] examined the neuronal activities by using codimension-two bifurcation and the theoretical calculation of Hopf bifurcation is simulated in the corresponding works.[22–24] Mixed-mode oscillations (MMOs) are a complicated case of the discharge rhythm pattern and they have been observed in an early work.[25] Some researchers[26–33] haveas illustrated the mechanism of MMOs in some respects, and it has been shown the existence of MMOs in folded node point of three-dimensional system with one fast and two slow variables[26] and there is an extension.[29]

In this paper, we investigate the complex dynamical behaviors and mixed-mode oscillations of the reduced model. First, we find that the time series of membrane potential can generate abundant bursting modes with the increasing of the membrane capacity C. There is an obvious period-adding that emerges via calculating inter-spike intervals (ISIs) sequence diagram. Furthermore, the transition of spiking pattern has been classified into three categories using slow–fast dynamics analysis that makes us to further understand the process of discharge from resting to firing or from firing to resting, and we have to determine whether it is subcritical or supercritical via calculating the first Lyapunov coefficient of Hopf bifurcation point. Moreover, codimension-two bifurcation of the fast subsystem is calculated to explore the bifurcation mechanism and exhibit the bifurcation diagram near the cusp. Mixed-mode oscillations emerge via adjusting related kinetic parameters simultaneously. Finally, we calculate the characteristic index, which is better to demonstrate the potential mechanism with the increasing of potassium conductance.

The paper is presented as follows. We describe the reduced model and elaborate the method in the numerical simulation in Sec. 2. In Sec. 3, there are three different bursting patterns, and we analyze the dynamical behaviors of discharge rhythm via using slow–fast dynamics analysis. We have to make an analysis by calculating codimension-two bifurcation. Related information about mixed-mode oscillation is addressed in Sec. 4. Finally, we conclude with a discussion in Sec. 5.

2. Model and Methods

We use a single-compartment model[1] that is developed by modifying the previous Purkinje model. The model contains sodium ion current, potassium ion current and leak current. The reduced two-equation nerve model is organized as

$$C\frac{dV}{dt} = I - g_{\mathrm{Na}} m_\infty(V)(1-n)(V-E_{\mathrm{Na}}) - g_{\mathrm{K}} n(V-E_{\mathrm{K}}) - g_{\mathrm{leak}}(V-E_{\mathrm{leak}}), \tag{1}$$

$$\frac{dn}{dt} = \frac{n_\infty - n}{\tau_n}, \tag{2}$$

where the steady-state gating functions are

$$m_\infty(V) = \frac{1}{\{1+\exp[-(V+35)/5]\}}, \quad n_\infty(V) = \frac{1}{\{1+\exp[-(V-V_2)/5]\}}.$$

The above system consists of Eqs. (1) and (2), variables V and n are the membrane voltage and the activation variable for potassium current, respectively. The parameters g_{K} and g_{Na} are the maximal conductances and g_{leak} is the leak conductance. E_{Na}, E_{K} and E_{leak} are the equilibrium potentials corresponding to the sodium, potassium and leak, respectively. Related parameters as follows: $C = 1.5\ \mu\mathrm{F/cm}^2$, $g_{\mathrm{Na}} = 20\ \mathrm{mS/cm}^2$, $g_{\mathrm{K}} = 4.2\ \mathrm{mS/cm}^2$, $g_{\mathrm{leak}} = 0.05\ \mathrm{mS/cm}^2$, $E_{\mathrm{Na}} = 45$ mV, $E_{\mathrm{K}} = -95$ mV, $E_{\mathrm{leak}} = -77$ mV, $V_2 = -36$ mV, $V_0 = -80$ mV and $\tau_n = 0.06$ ms.

Now our idea is to add the external stimuli current I as a linear control equation of voltage feedback satisfying

$$\frac{dI}{dt} = \epsilon(V_0 - V), \tag{3}$$

where ϵ acts in the role of feedback coefficient. And in the following computation, we take $\epsilon = 0.001$. V_0 is an alterable parameter.

Equations (1)–(3) are called reduced system of cerebellar Purkinje cells with the current of voltage-feedback control. Obviously, it contains two fast variables and one slow variable, which are required to develop a bursting behavior and there are complex nonlinear dynamical properties in the reduced system since the steady-state gating functions are nonlinear functions of the membrane potential V.

The mathematical mechanism of firing can have a pretty good continuation from the five-equation model, which is similar to the two-equation model that possesses abundant dynamical behaviors and is able to establish bistability. The firing mechanism of the system is affected by the interaction between the fast subsystem and the slow subsystem. The time scale of this system is interpreted as follows: a faster subsystem be controlled by sodium and potassium, which can exhibit a number of different states such as resting, period-bursting and period-spiking, and a slow subsystem can be shown to adjust the fast subsystem by its regular periodic oscillatory and quiescent states in a quasi-static manner. The slow-varying dynamical behavior can be effected greatly by the intracellular calcium-dependent or other slow

voltage-dependent processes.[34] The feedback current I that is voltage-dependent in Eq. (3) is the slow variable of the entire system. Because ϵ is very small, it has a better adjustment for Eqs. (1) and (2) and is used to analyze the essence of bifurcation of the fast subsystem.[26,27,29,32] We will study the functions of both the inward current of the system and maximal conductance and the firing mechanism of bursting-mode oscillations.[19]

In this paper, we can describe the firing behavior and draw the ISI bifurcation diagrams of membrane potentials of this system by using matplotlib which is the package in Python. The firing number can be computed using MATLAB, and the codimension-one and codimension-two bifurcation diagrams are calculated applying the MATCONT software. We adopt fourth-order Runge–Kutta algorithm in all of numerical simulations and in order to avoid the effects of the initial value, we discard the first 4000 ms.

3. Analysis of Bifurcation Behavior

In neurons, there are many important biological information that are encoded by membrane capacitance, which can propagate different biological signals by varying the electrical signal of the membrane voltage. The membrane capacitance is not the same in different parts of the same cell, not to mention the different parts of different cells. Therefore, we investigate the membrane capacitance that seems to be more significant. Similarly, changing the external stimuli has an active effect on neuronal discharge.

In order to investigate the different spike-adding transition modes, we demonstrate the ISI bifurcation diagrams by changing the membrane capacitance C, from which we are able to accurately observe the process of transition. It plays a very important role in strengthening the understanding of dynamical behavior. Next, we will explore the bifurcation analysis of the system via adjusting external stimuli and kinetic parameters.

3.1. *Elaborate bursting mechanism via two fast/one slow dynamics analysis*

Many dynamical properties are demonstrated as the focus of investigation by slow–fast dynamical bifurcation analysis, then we have obtained three bursting types in our calculation using the same method. It has significant construction in the bursting generation and disappearance.

3.1.1. *The "supHopf/homoclinic" bursting via "fold/homoclinic" hysteresis loop*

We use the fourth-order Runge–Kutta algorithm to simulate the system, and then we obtain the pseudo-plateau bursting, which is exhibited in Fig. 1(a) for $C = 2.5\ \mu\text{F/cm}^2$. We can draw the bifurcation curve of fast subsystem, which has a

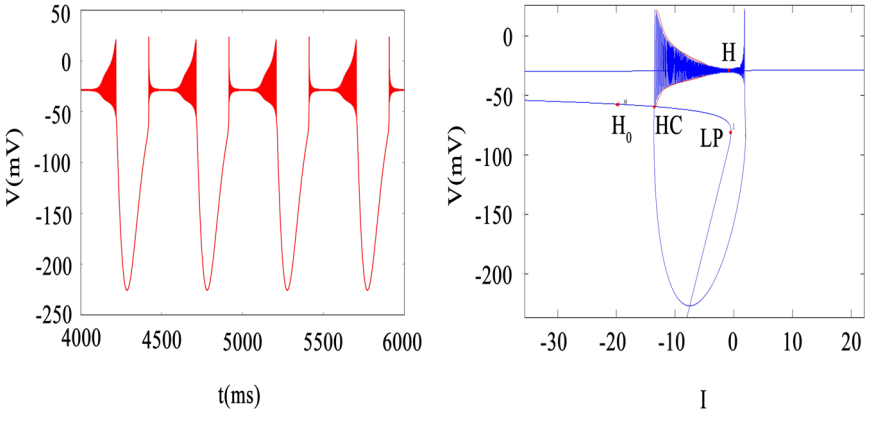

(a) (b)

Fig. 1. (Color online) The "supHopf/homoclinic" bursting discharge mechanism via "fold/homoclinic" hysteresis loop for $C = 2.5\ \mu\text{F/cm}^2$. (a) The bursting of membrane potential; and (b) dynamical behavior of the fast subsystem.

bistability that is up-state resting and down-state quiescence. As shown in Fig. 1(b), there is just one Hopf bifurcation point H in up-state resting, which consists of stable focus. Following, we can observe that the stable limit cycle emerges via the Hopf bifurcation point H. The solid red line denotes the minimum and maximum values of limit cycle. The middle and lower branches of the bifurcation curve represent the saddle and node, respectively.

In order to determine whether the Hopf bifurcation point H is supercritical or not, we will calculate the first Lyapunov coefficient at the Hopf bifurcation point.[35,36] With this idea, we rewrite the fast subsystem of the system as follows:

$$\begin{cases} \dfrac{dV}{dt} = f_1(V, n, I), \\ \dfrac{dn}{dt} = f_2(V, n, I), \end{cases} \tag{4}$$

where

$$\begin{aligned} f_1 = \frac{1}{C}\{&I - g_{\text{Na}} m_\infty(V)(1-n)(V - E_{\text{Na}}) \\ &- g_{\text{K}} n(V - E_{\text{K}}) - g_{\text{leak}}(V - E_{\text{leak}})\}, \\ f_2 = \frac{n_\infty(V) - n}{\tau_n}. \end{aligned}$$

The Jacobian matrix A of the system can be written as

$$A = \begin{pmatrix} \dfrac{\partial f_1}{\partial V} & \dfrac{\partial f_1}{\partial n} \\ \dfrac{\partial f_2}{\partial V} & \dfrac{\partial f_2}{\partial n} \end{pmatrix},$$

where

$$\begin{aligned}
\frac{\partial f_1}{\partial V} &= \frac{1}{C}\{-g_{\mathrm{Na}} m_\infty(V)(1-n) \\
&\quad - g_{\mathrm{Na}} \dot{m}_\infty(V)(1-n)(V-E_{\mathrm{Na}}) - g_{\mathrm{K}} n - g_{\mathrm{leak}}\}, \\
\frac{\partial f_1}{\partial n} &= g_{\mathrm{Na}} m_\infty(V)(V-E_{\mathrm{Na}}) - g_{\mathrm{leak}}, \\
\frac{\partial f_2}{\partial V} &= \frac{\dot{n}_\infty(V)}{\tau_n}, \\
\frac{\partial f_2}{\partial n} &= \frac{-1}{\tau_n},
\end{aligned}$$

where "$\cdot$" indicates the derivative with respect to V.

When $I = -3.374737$ mA, the fast subsystem has an equilibrium point that is $(-29.076620,\ 0.799741)$. Correspondingly, the eigenvalues of the matrix A at the equilibrium point are $\lambda_{1,2} = \pm 7.6167i$. Therefore, the Hopf bifurcation of the fast subsystem occurs.

Following, the first Lyapunov coefficient can be calculated at the point H to determine whether it is supercritical bifurcation point or not. At the equilibrium point, Jacobian matrix A can be rewritten as

$$A|_H = \begin{pmatrix} 1.666665 & -1138.739021 \\ 0.053385 & -1.666667 \end{pmatrix}$$

with a pair of conjugate pure imaginary roots λ, $\bar{\lambda}$ and $\lambda = iw$, where $w = 7.6167$. $q = (1, 0.0015 - 0.0067i)^T$ is an eigenvector of eigenvalue λ, which satisfies $Aq = \lambda q$ and $A\bar{q} = \bar{\lambda}\bar{q}$, and the adjoint eigenvector p satisfies $A^T p = \bar{\lambda} p$ and $A^T \bar{p} = \lambda \bar{p}$. And the normalization $\langle p, q\rangle = 1$, here $\langle p, q\rangle = \bar{p}_1 q_1 + \bar{p}_2 q_2$ is the standard scalar product in $\mathbb{C}^2$. Hence, we can take it as $p = (0.5 + 0.1119i, -74.6269i)^T$.

Consider the system

$$\dot{x} = Ax + F(x), \quad x \in R^2,$$

where $F(x)$ is a smooth vector function and $F(x) = O(\|x\|^2)$. A is a Jacobian matrix at the equilibrium point. $F(x)$ can be rewritten as

$$F(x) = \frac{1}{2}B(x,x) + \frac{1}{6}C(x,x,x) + O(\|x\|^4),$$

where $B(x, y)$ and $C(x, y, u)$ are multiple linear vector functions and $x = (x_1, x_2)^T$, $y = (y_1, y_2)^T$ and $u = (u_1, u_2)^T$.

Specifically, we have

$$B_i(x,y) = \sum_{j,k=1}^{2} \left.\frac{\partial^2 F_i(\xi)}{\partial \xi_j \partial \xi_k}\right|_{\xi=\xi_0} x_j y_k, \quad i = 1, 2,$$

$$C_i(x,y,u) = \sum_{j,k,l=1}^{2} \left.\frac{\partial^3 F_i(\xi)}{\partial \xi_j \partial \xi_k \partial \xi_l}\right|_{\xi=\xi_0} x_j y_k u_l, \quad i = 1, 2,$$

where $\xi = (\xi_1, \xi_2)^T$ and ξ_0 is the equilibrium point.

We write the fast subsystem as

$$\begin{pmatrix} \dot{V} \\ \dot{n} \end{pmatrix} = A|_H \begin{pmatrix} V \\ n \end{pmatrix} + \begin{pmatrix} F_1(V,n) \\ F_2(V,n) \end{pmatrix}, \tag{5}$$

where

$$\begin{aligned} F_1(V,n) &= \{-3.374737 - 20m_\infty(V)(1-n)(V-45) - 4.2n(V+95) \\ &\quad - 0.05(V+77)\}/2.5 - 1.666665V + 1138.739021n, \\ F_2(V,n) &= 1.666667n_\infty(V) - 0.053385V, \\ m_\infty(V) &= 1/\{1+\exp[-(V+35)/5]\}, \\ n_\infty(V) &= 1/\{1+\exp[-(V-V_2)/5]\}. \end{aligned}$$

Therefore, we have

$$B(x,y) = \begin{pmatrix} 0.567528x_1y_1 + 13.4515558(x_1y_2 + x_2y_1) \\ -0.00640068x_1y_1 \end{pmatrix},$$

$$C(x,y,u) = \begin{pmatrix} -0.005364x_1y_1u_1 - 2.833971(x_1y_1u_2 + x_1y_2u_1 + x_2y_1u_1) \\ 0.000083x_1y_1u_1 \end{pmatrix},$$

$$\begin{aligned} g_{20} &= \langle p, B(q,q)\rangle = 0.324112 + 0.455560i, \\ g_{11} &= \langle p, B(q,\bar{q})\rangle = 0.303941 + 0.545685i, \\ g_{21} &= \langle p, C(q,q,\bar{q})\rangle = -0.011183 - 0.001241i. \end{aligned}$$

The first Lyapunov coefficient at the Hopf bifurcation point can be calculated as

$$l_1(0) = \frac{1}{2w^2}\mathrm{Re}(ig_{20}g_{11} + wg_{21}) = -0.0034 < 0.$$

Hence H is a supercritical Hopf bifurcation point and is able to branch out the only stable limit cycle.

Therefore, we can see that the transition appears from down-state quiescence to up-state and gradually decays to resting state via Hopf bifurcation H, although there exists a fly in the ointment. Then the bifurcation of bursting and stable limit cycle emerges via the Hopf bifurcation point H. Bursting will be continued until it hits the saddle point of the middle branch of bifurcation curve, and then the up-state bursting returned to down-state resting via saddle homoclinic bifurcation. Thus, the bursting pattern is known as "supHopf/homoclinic" bursting via "fold/homoclinic" hysteresis loop in the works of Izhikevich.[8,11]

3.1.2. *The "circle/homoclinic" bursting via "circle/homoclinic" hysteresis loop*

Figure 2(a) illustrates the spiking pattern of the reduced model when $C = 1.0\ \mu\text{F/cm}^2$. A part of S-shaped bifurcation curve and the (I, V) phase plane of the whole system are superimposed together in Fig. 2(b). It is only considered that the slow variable is in a very small range. We can calculate that there exists only one supercritical Andronov–Hopf bifurcation point H on the upper branch of the S-shaped bifurcation curve of the fast subsystem at $I = 37.594729$. With the decreasing of I, the point on the bifurcation curve changes from stable focus to unstable focus and a stable limit cycle emerges via Hopf bifurcation H. The point H_0 on the middle branch is a neutral saddle, not the Andronov–Hopf bifurcation point. The middle and lower branches of the S-shaped bifurcation curve are occupied by saddle and node, respectively. As shown in Fig. 2(c), stable limit cycle passes through precisely the fold LP and hence it has to become a saddle–node homoclinic orbit. The red line represents the minimum and maximum values of limit cycle, while green and blue lines represent nullclines of the variables n and V, respectively.

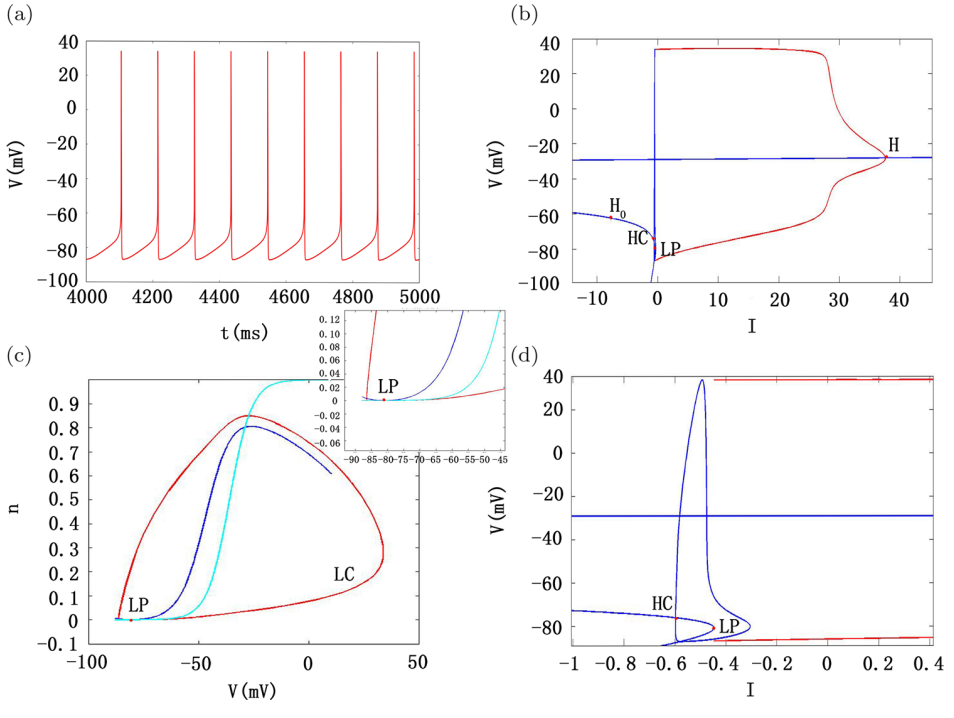

Fig. 2. (Color online) The "circle/homoclinic" bursting discharge mechanism via "circle/homoclinic" hysteresis loop for $C = 1.0\ \mu\text{F/cm}^2$. (a) Time course of membrane potential; (b) slow–fast dynamical bifurcation analysis for the fast subsystem; (c) the limit cycle passing through the saddle–node; and (d) an enlarged view of the portion of (b). The supercritical Hopf bifurcation is denoted by H, the neutral saddle is denoted by H_0, LP represents the fold bifurcation, HC represents the saddle homoclinic orbit and limit cycle is denoted by LC.

We explicate the discharge mechanism using Fig. 2(d). Resting state transits to the bifurcation of spiking state via saddle–node bifurcation on the invariant circle, then the spiking state returns to resting state via the saddle homoclinic bifurcation. Corresponding to the classification of slow–fast dynamical analysis,[8,11] the type is "circle/homoclinic" bursting. Therefore, the bursting pattern is shown as "circle/homoclinic" bursting via "circle/homoclinic" hysteresis loop.

3.1.3. *The "fold/homoclinic" bursting via "fold/homoclinic" hysteresis loop*

Figure 3(a) exhibits another spiking mode for $C = 1.5\ \mu\text{F/cm}^2$. Li and Gu[37] have recently studied the bursting mode and show the distinct stochastic and deterministic dynamics between period-adding and period-doubling bifurcations. It is differentiated from the above, although there is no difference from our intuitive sense. Similarly, Fig. 3(b) only shows a part of S-shaped bifurcation curve of the fast subsystem. Using the same method as above, we can see that there exists a supercritical Hopf bifurcation point H in the upper branch of the S-shaped bifurcation curve at $I = 22.9812621$. The middle and lower branches of the S-shaped

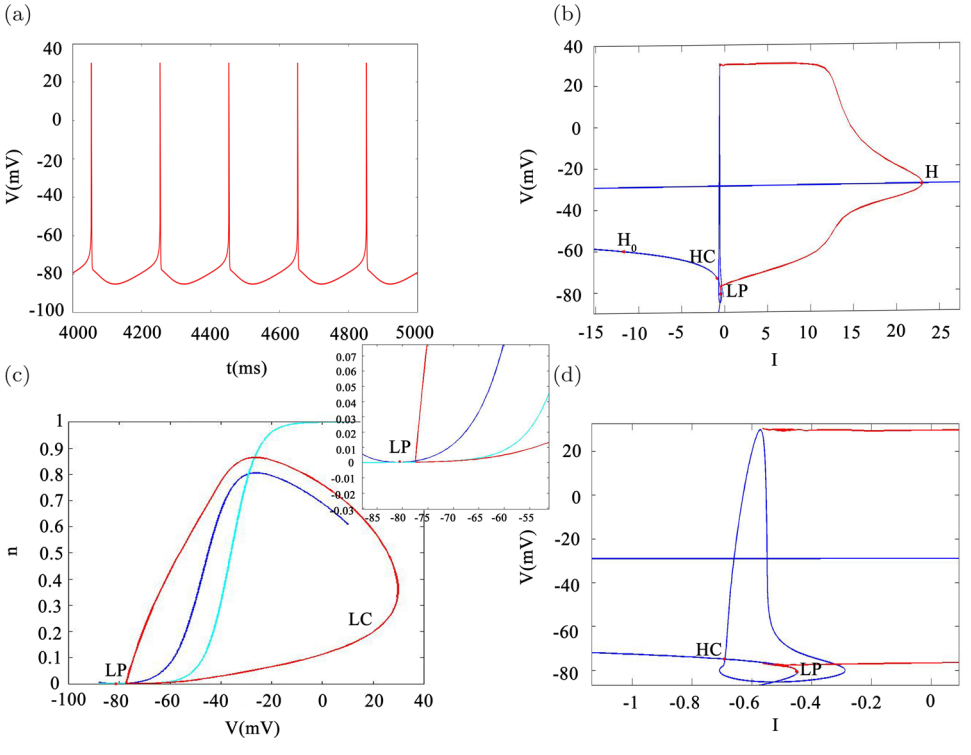

Fig. 3. (Color online) The "fold/homoclinic" bursting discharge mechanism via "fold/homoclinic" hysteresis loop for $C = 1.5\ \mu\text{F/cm}^2$. (a) Time series of membrane potential; (b) the bifurcation curve of the fast subsystem; (c) limit cycle deviation from the saddle–node; and (d) an enlarged view of the portion of (b).

bifurcation curve are occupied by saddle and node, respectively. The stable limit cycle appears via the Hopf bifurcation point H with the decreasing of I, and we can know that the saddle–node point deviates from the orbit of limit cycle as shown in Fig. 3(c). The solid red line represents the minimum and maximum values of stable limit cycle.

There exists a fly in the ointment because the (I, V) phase plane is not containing the fold LP. But also the stable limit cycle appears when the resting state transits to the spiking state via the fold bifurcation LP (quiescence via saddle–node homoclinic bifurcation). The limit cycle is involved to hit a saddle point and it forms the saddle homoclinic bifurcation orbit while making the firing state return to the resting state. Thus, the bursting pattern shows the category as "fold/homoclinic" bursting via "fold/homoclinic" hysteresis loop.

3.2. *Codimension-two analysis for planar system*

In Fig. 4, the supercritical Hopf bifurcation curve supH_1 is tangential to the fold bifurcation curve F_2 at codim-2 Bogdanov–Takens bifurcation point BT(-2.519583,

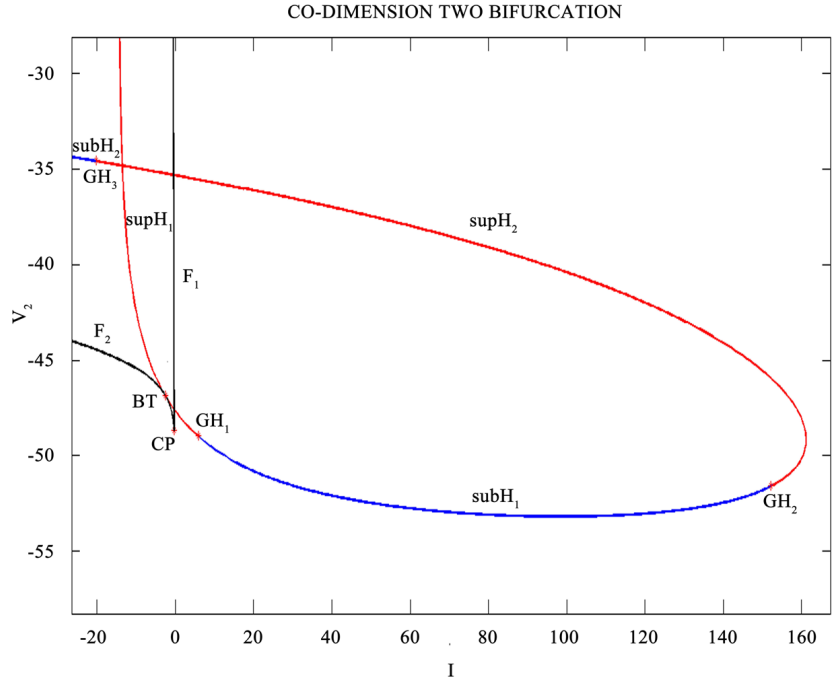

Fig. 4. (Color online) Codimension-two bifurcation of the fast subsystem. The labels are described as below: the Bogdanov–Takens and cusp are denoted by BT and CP, respectively; GH_i $(i = 1, 2, 3)$ represents the generalized Hopf (Bautin). The sup$H$ and sub$H$ stand for supercritical Hopf bifurcation and subcritical Hopf bifurcation, respectively. The fold bifurcation curves are denoted by F_1 and F_2.

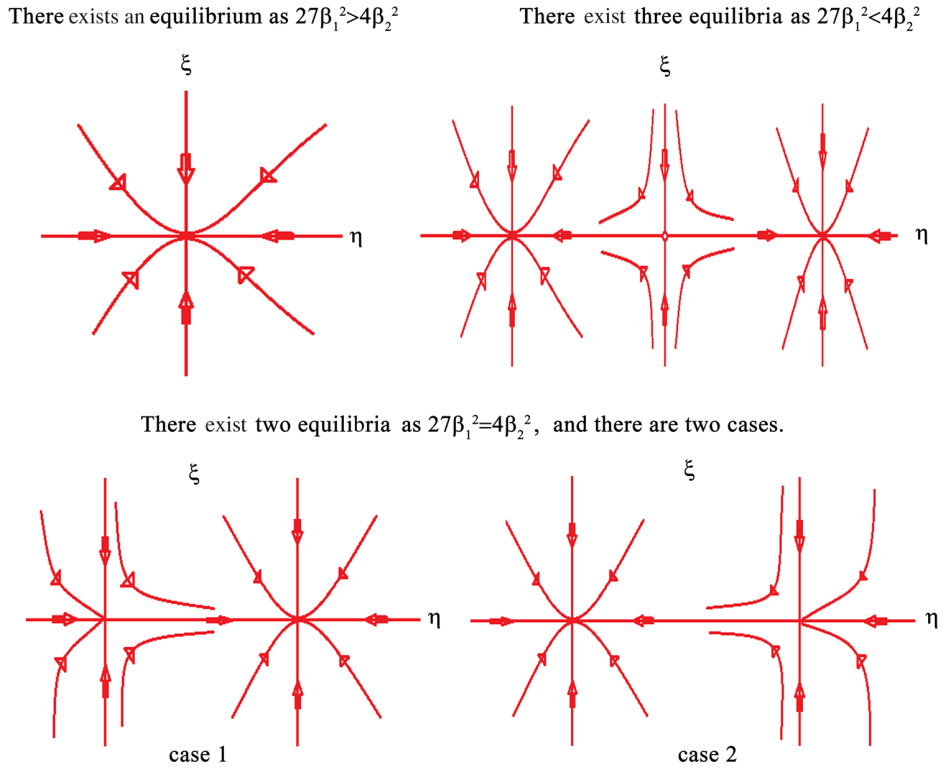

Fig. 5. (Color online) The sketchy diagrams of cusp bifurcation.

-46.837855) and it terminated the point of BT. The fast subsystem is locally topologically equivalent near the equilibrium to normal forms:

$$\begin{cases} \dot{\eta}_1 = \eta_2, \\ \dot{\eta}_2 = \beta_1 + \beta_2\eta_1 + {\eta_1}^2 + s\eta_1\eta_2, \end{cases} \tag{6}$$

where $a = -0.05537816$, $b = 0.2818546$, $s = \text{sign}(ab) = -1$, $\eta_{1,2} \in R^1$ and $\beta_{1,2} \in R$.

The CP$(-0.262305, -48.688284)$ is the intersection point of the fold bifurcation curves F_1 and F_2. Near the equilibrium (eigenvalues $\lambda_1 = 0$ and $\lambda_2 = -1.56631$), it is locally topologically equivalent to the following normal forms:

$$\begin{cases} \dot{\eta} = \beta_1 + \beta_2\eta + s\eta^3, \\ \dot{\xi} = -\xi, \end{cases} \tag{7}$$

where $c = -0.0002709506$, $s = \text{sign}(c) = -1$, $\eta \in R^1$, $\xi \in R^1$ and $\beta_{1,2} \in R$.

We provide the sketches of bifurcation diagrams near the cusp in Fig. 5.[35]

4. Generation of Mixed-Mode Oscillation

By varying the original data, we find that the bursting discharge pattern is considerably rich in terms of the numerical simulated results under the current parameters.

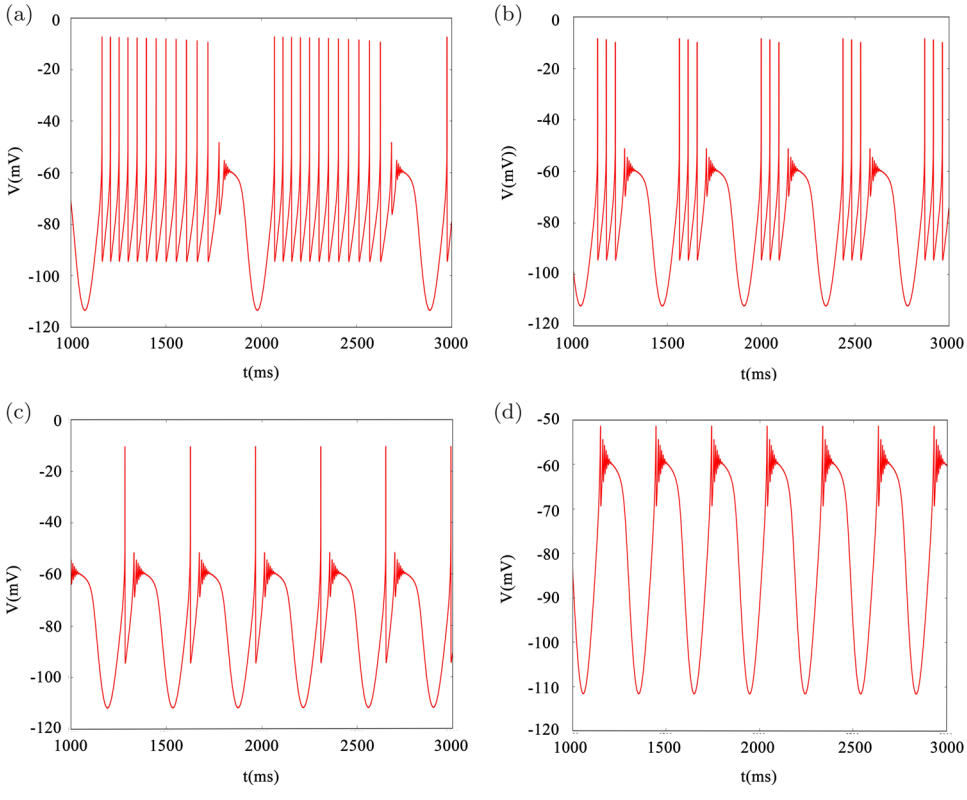

Fig. 6. (Color online) Time series of membrane voltages of mixed-mode oscillations. Panels (a)–(d) are for $g_K = 46.0$, 46.5, 46.7 and 46.8 mS/cm^2, respectively, with $g_{leak} = 0.01$ mS/cm^2 and $C = 1.75$ μF/cm^2.

Dynamical properties of mixed-mode oscillation are investigated in many neuronal models and chemical systems.[25,27,38] As shown in Fig. 6, different mixed-mode oscillation patterns are simulated with the change of potassium conductance. With the increasing of conductance g_K, the large-amplitude oscillations are gradually decreased while the small-amplitude oscillations are gradually increased. Especially, there is a 12^6 MMO pattern when $g_K = 46.0$ mS/cm^2, that is to say that the relaxation oscillation is twice the small-amplitude oscillation. When $g_K = 46.5$ mS/cm^2, the electrical activity has a 3^7 MMO mode. With the further increase of g_K, 1^7 MMO pattern can be observed until $g_K = 46.7$ mS/cm^2. Relaxation oscillation disappears when $g_K = 46.8$ mS/cm^2. This terminology is illustrated in related literatures,[39,40] relaxation oscillations are corresponding to spiking of membrane potentials while small-amplitude oscillations are corresponding to subthreshold oscillations. There exists a rich transition of bursting mode from Fig. 6(a) to Fig. 6(d) but we are interested in this detailed process of change.

In order to investigate the process of electrical activities, we can define the firing number[25] as $F = S/(S + L)$ where L^s represents L large oscillations (spiking value

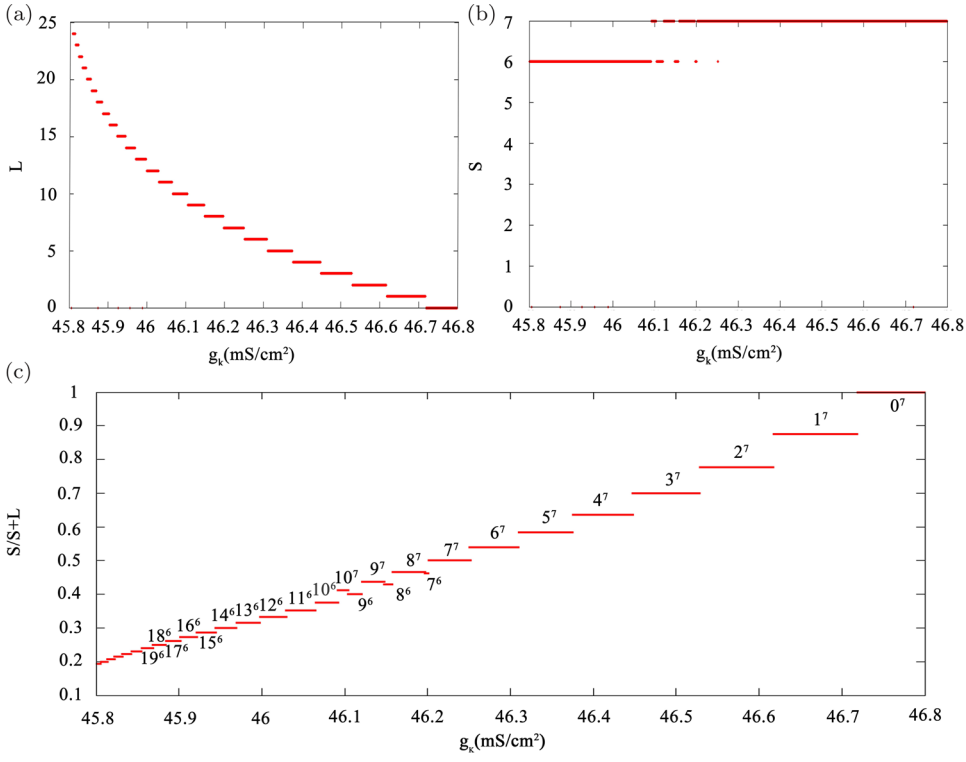

Fig. 7. (Color online) Firing number $F = S/(S+L)$ (Devil's staircase). L stands for the number of large-amplitude oscillations while S stands for the number of small-amplitude oscillations when g_{K} is a fixed value.

is greater than the pre-value of -40 mV) followed by S small oscillations (spiking value is less than the pre-value of -40 mV) and calculate firing number to make a detailed illustration. In Fig. 7, we exhibit the bifurcation diagram, which corresponds to the mixed-mode action potentials consisting of relaxation oscillations and small-amplitude oscillations. Therefore, we can summarize the transition mode of MMOs in the system by the changing of firing number. With the increase of potassium conductance, the firing number of MMOs remains stable in some intervals and shows a rising staircase, which is the characteristic index and can clearly express the relationship between relaxation oscillations and small-amplitude oscillations. We can see that there exists an oscillation mode 0^7 consisting of seven small-amplitude oscillations and no existing large oscillations for $g_{\mathrm{K}} = 46.8$ mS/cm^2. The oscillation mode can be transferred to other stable bursting discharge with the decreasing of potassium conductance. Then L^7 and L^6 ($L = 7, 8, 9, 10$) mixed-oscillation modes will alternately appear until $g_{\mathrm{K}} = 46.1$ mS/cm^2 and then there is a stable interval for the electrical activity before the alternation begins. Moreover, it tends to six small-amplitude oscillations followed by the increasing of large oscillations, and finally mixed-mode oscillation disappears and only the spiking emerges

for $g_K = 45.7$ mS/cm^2. We can obtain this new phenomenon at the critical value $g_K = 45.7$ mS/cm^2, then dynamical properties may be adjusted in this neighborhood. This process is accompanied by a steady change in small oscillations and a continuous increase in large oscillations until mixed-mode oscillations disappear. And relaxation oscillations transit to the spiking via chaotic region while small oscillations vanish in terms of the result of numerical simulation. The potassium conductance g_K plays a vital role in the transition, hence it is strongly necessary that we investigate the conductance g_K.

5. Conclusions

Purkinje cells are only an efferent nerve to propagate action potentials starting from cerebellar cortex. It is closely linked to certain diseases of mammals, and is mainly associated with regenerative medicine. As a way of encoding information, bursting and spiking can well describe the electrical activities of neurons. Therefore, for this reduced Purkinje cell model, we have analyzed the electrical activities using the original parameters via numerical simulation. Then, a detailed decomposition is given. In this paper, we have drawn the time course of membrane potential, and obtained various bursting patterns such as period-2, period-6, square-wave bursting, pseudo-plateau bursting and so on. These bursting modes show the behavior from spiking to chaos with the process of spike-adding. In addition, three typical bursting patterns are discovered to illustrate the generation mechanism of spiking via using slow–fast dynamics analysis. These three types of bursting are "supHopf/homoclinic" bursting via "fold/homoclinic" hysteresis loop, "circle/homoclinic" bursting via "circle/homoclinic" hysteresis loop and "fold/homoclinic" bursting via "fold/homoclinic" hysteresis loop. Moreover, we have drawn the bi-parameters bifurcation diagrams and made an analysis to further understand the dynamical behaviors of the fast subsystem via exhibiting the bifurcation diagram near the cusp. Finally, time series of mixed-mode oscillations have been shown in the paper, and mathematical mechanism is distinctive with different large and small oscillations. The firing number reflects well the transition of the relaxation oscillations and small oscillations, and it demonstrates deeply the hidden properties in the Devil's staircase. In addition to the properties we have investigated, it is still possible to obtain abundant dynamical behavior with a variety of multiparameters, and that may be considered in our future work.

Acknowledgments

This work was supported by the National Natural Science Foundation of China under Grant Nos. 11172103 and 11572127.

References

1. F. R. Fernandez, J. D. Engbers and R. W. Turner, *J. Neurophysiol.* **98**, 278 (2007).
2. Y. Loewenstein *et al.*, *Nat. Neurosci.* **8**, 202 (2005).

3. J. Ma, F. Wu and C. Wang, *Int. J. Mod. Phys. B* **31**, 1650251 (2016).
4. Y. B. Jia and H. G. Gu, *Int. J. Mod. Phys. B* **29**, 1550142 (2015).
5. Y. Xu, W. Jin and J. Ma, *Int. J. Mod. Phys. B* **29**, 1550164 (2015).
6. J. Ma *et al.*, *Int. J. Mod. Phys. B* **29**, 1450239 (2014).
7. Y. Q. Che *et al.*, *Int. J. Mod. Phys. B* **28**, 1450114 (2014).
8. E. M. Izhikevich, *Int. J. Bifurcatian Chaos* **10**, 1171 (2000).
9. E. M. Izhikevich, *Dynamical Systems in Neuroscience: The Geometry of Excitability and Bursting* (MIT Press, Cambridge, 2007).
10. E. M. Izhikevich *et al.*, *Trends Neurosci.* **26**, 161 (2003).
11. E. M. Izhikevich and F. Hoppensteadt, *Int. J. Bifurcatian Chaos* **14**, 3847 (2011).
12. J. Wang *et al.*, *Int. J. Bifurcatian Chaos* **25**, 1530024 (2015).
13. B. Lu *et al.*, *Int. J. Bifurcatian Chaos* **26**, 05 (2016).
14. Z. Q. Yang and Q. S. Lu, *Sci. China G* **51**, 687 (2008).
15. Z. Q. Yang and Q. S. Lu, *Commun. Nonlinear Sci. Numer. Simul.* **12**, 357 (2007).
16. X. L. Liu and S. Q. Liu, *Nonlinear Dyn.* **67**, 847 (2012).
17. H. Wang, Q. Lu and Q. Wang, *Commun. Nonlinear Sci. Numer. Simul.* **13**, 1688 (2008).
18. Z. G. Zhao, B. Jia and H. Gu, *Nonlinear Dyn.* **86**, 1 (2016).
19. J. Rinzel and B. Ermentrout, in *Methods in Neuronal Modeling* (MIT Press, Cambridge, MA, 1998), 251–291.
20. Y. Che *et al.*, *Int. J. Mod. Phys. B* **28**, 5447 (2014).
21. Z. G. Zhao and H. G. Gu, *Sci. Rep.* **7**, 6760 (2017).
22. D. Fan, L. Hong and J. Wei, *Nonlinear Dyn.* **62**, 305 (2010).
23. C. Huang *et al.*, *Nonlinear Dyn.* **87**, 755 (2017).
24. J. Wang *et al.*, *Int. J. Bifurcatian Chaos* **27**, 1750010 (2017).
25. V. Petrov, S. Scott and K. Showalter, *J. Chem. Phys.* **97**, 6191 (1992).
26. M. Wechselberger, *SIAM J. Appl. Dyn. Syst.* **4**, 101 (2005).
27. M. Desroches *et al.*, *SIAM Rev.* **54**, 211 (2012).
28. M. Wechselberger, J. Mitry and J. Rinzel, *Lect. Notes Math.* **21**, 89 (2013).
29. M. Brons, M. Krupa and M. Wechselberger, *Fields Inst. Commun.* **49**, 39 (2006).
30. P. Szmolyan and M. Wechselberger, *J. Differ. Equ.* **177**, 419 (2001).
31. M. Wechselberger and W. Weckesser, *Physica D* **238**, 1598 (2009).
32. F. A. Homles, *Singular-Perturbation Theory: An Introduction with Application* (Cambridge University Press, Cambridge, 1985).
33. N. Fenichel, *J. Differ. Equ.* **31**, 53 (1979).
34. R. M. Ghigliazza and P. Holmes, *SIAM J. Appl. Dyn. Syst.* **3**, 636 (2004).
35. Y. A. Kuznetsov, *Elements of Applied Bifurcation Theory* (Springer-Verlag, New York, 1998).
36. M. Sterpu and C. Rocsoreanu, *Nonlinear Anal., Real World Appl.* **6**, 1 (2005).
37. Y. Y. Li and H. G. Gu, *Nonlinear Dyn.* **87**, 2541 (2017).
38. H. G. Rotstein, *Enc. Comput. Neurosci.* **2**, 1 (2014).
39. H. G. Rotstein *et al.*, *J. Comput. Neurosci.* **21**, 271 (2006).
40. J. Rubin and M. Wechselberger, *Chaos* **18**, 5 (2008).